Optimisation of the Size and Cost of Heliostats in a Concentrating Solar Thermal Power Tower Plant

Matthew Emes, The University of Adelaide, Australia
Farzin Ghanadi, The University of Adelaide, Australia
Maziar Arjomandi, The University of Adelaide, Australia
Richard Kelso, The University of Adelaide, Australia

The European Conference on Sustainability, Energy & the Environment 2017
Official Conference Proceedings

Abstract
Concentrating solar thermal (CST) power tower (PT) is one of the most promising renewable technologies for large-scale electricity production, however the main limitation of PT systems is their significantly larger levelised cost of electricity (LCOE) relative to base load energy systems. One opportunity to lower the LCOE is to reduce the capital cost of heliostats through optimisation of the size and position of heliostat mirrors to withstand maximum wind loads during high-wind conditions when aligned parallel to the ground in the stow position. Wind tunnel experiments were carried out to measure the forces on thin flat plates of various sizes at a range of heights in a simulated part-depth atmospheric boundary layer (ABL). Calculated peak wind load coefficients on the stowed heliostat showed an inverse proportionality with the chord length of the heliostat mirror, which suggests that the coefficients could be optimised by increasing the size of the heliostat mirror relative to the sizes of the relevant eddies approaching the heliostat. The peak lift coefficient and peak hinge moment coefficient on the stowed heliostat could be reduced by as much as 23% by lowering the elevation axis height of the heliostat mirror by 30% in the simulated ABL. A significant linear increase of the peak wind load coefficients occurred at longitudinal turbulence intensities greater than 10% in the simulated ABL. Hence, the critical scaling parameters of the heliostat should be carefully considered depending on the turbulence characteristics of the site.

Keywords: heliostat, stow position, turbulence, atmospheric boundary layer

iafor
The International Academic Forum
www.iafor.org

Introduction

Current energy systems, based primarily on the combustion of fossil fuels, are unsustainable in the long term, so that a transition to an environmentally-sustainable energy system with the integration of renewable energy sources is necessary (Hernández-Moro & Martínez-Duart, 2012). Concentrating solar thermal (CST) is one of the most promising renewable technologies capable of large scale electricity production (Hinkley et al., 2013). A CST system operates by focusing direct solar radiation to obtain higher energy densities and thus an improved Carnot efficiency at higher temperatures. Heat collected in the receiver is typically used to heat a working fluid to generate supercritical steam that drives a turbine for electricity generation (IRENA, 2015); although a wide range of alternative power cycles is under development including Brayton and CO_2 power cycles. Parabolic trough systems are the most commercially-deployed CST technology, however power tower (PT) systems have been identified as an emerging concept that can operate at higher concentration ratios and higher working fluid temperatures than parabolic troughs, thus allowing for higher power cycle efficiency (IEA-ETSAP & IRENA, 2013). Although the intermittency of solar irradiation is a practical limitation of CST systems, PT plants can be deployed with thermal energy storage or as a hybrid system with existing fossil fuel power plants for a base-line power supply (Hinkley et al., 2013; Kolb, Ho, Mancini, & Gary, 2011).

The main limitation of PT systems is their significantly larger levelised cost of electricity (LCOE), in the range of 0.15-0.19 USD/kWh in 2015 (IRENA, 2015), compared to base-load energy systems such as fossil fuel power plants in the range of 0.06-0.13 USD/kWh in 2011 (IRENA, 2013). To reduce the LCOE of PT systems there is a need to lower the capital cost of a PT plant, of which the largest cost is the heliostat field, with an estimated contribution of between 40% and 50% (Coventry & Pye, 2014; Hinkley et al., 2013; IRENA, 2015; Kolb et al., 2007). Government-funded initiatives that support the research and development of CST systems to make them competitive with base-load energy rates include the SunShot Initiative by the Department of Energy (DOE) in the USA, with a goal LCOE of 0.06 USD/kWh by 2020 (Kolb et al., 2011), and the Australian Solar Thermal Research Initiative (ASTRI) targeting a LCOE of 0.12 AUD/kWh by 2020. Currently, the total installed cost of a 150 MW PT plant is 5700 USD/kW. Figure 1 shows that the total cost of PT plants is projected to be reduced by 37% to 3600 USD/kW by 2025, compared with a projected 33% reduction in parabolic troughs (IRENA, 2015). The largest reduction of 24% in the cost of the solar field is expected to be achieved through the optimisation of the structural design of heliostats to wind loading. Hence, the aim of this paper is to optimise the size and cost of heliostats to withstand the maximum wind loads during high-wind conditions in the stow position.

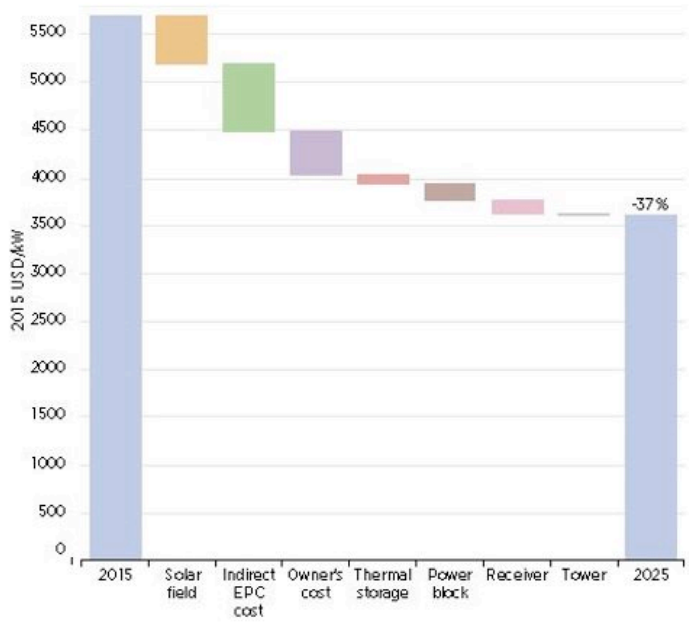

Figure 1: Projected reduction in capital cost (USD/kW) of a 150 MW PT plant from 2015 to 2025 (IRENA, 2015).

Kolb et al. (2007) concluded that the optimum heliostat size for a molten-salt PT plant is between 50 m^2 and 150 m^2, however there is no consensus on the optimal size of a heliostat mirror. This is because the optimum heliostat size is dependent on many factors associated with the production volume and manufacturing processes, ease of access to the electricity network in the region and the terrain type and wind conditions at the site. Therefore, further understanding of the relationships between the heliostat cost and the wind loading on heliostats needs to be developed. One opportunity to lower the heliostat cost is through optimisation of the size and position of heliostat mirrors to withstand maximum wind loads during high-wind conditions. Heliostats are aligned parallel to the ground in the stow position during periods of high wind speeds to minimise the frontal area and the large drag forces that the heliostat are exposed to in operating positions, however stowed heliostats must withstand maximum lift forces and hinge moments due to the effects of vortex structures embedded within the turbulence in the atmospheric boundary layer. The motor drives, support structure and mirror must all withstand any forces and moments, applied to the heliostat from the wind. These wind-sensitive structural components account for up to 80% of the heliostat capital cost according to research by Kolb et al. (2011). A cost analysis of quasi-static wind loads on individual heliostat components by Emes, Arjomandi, and Nathan (2015) found that the sensitivity of the total heliostat cost to the stow design wind speed increased by 34% for an increase in mean wind speed from 10 m/s to 15 m/s. Following the linear cost-load proportionality developed by McMaster Carr, a 40% reduction in the peak hinge moment on the elevation drive of a conventional heliostat can lead to a 24% saving in the representative gear reducer cost (Lovegrove & Stein, 2012). Hence, this paper investigates the effect of the critical scaling parameters of the heliostat on the peak wind loads in stow position.

Methodology

Experimental measurements were taken in a closed-return wind tunnel at the University of Adelaide. Figure 2 shows the test section of the tunnel with a development length of 17 m and a cross-section expanding to 3 m × 3 m to allow for a pressure gradient resulting from growth of the boundary layer. The tunnel can be operated at speeds of up to 20 m/s with a low level of turbulence intensity, ranging between 1% and 3%. Accurate representation of a part-depth ABL in the wind tunnel is required to replicate similar turbulence properties that heliostats are exposed to in the lower surface layer of the ABL, including a logarithmic mean velocity profile. It is generally accepted that the most effective wind tunnel simulation of the ABL is obtained when a flow passes over a rough surface producing a natural-growth boundary layer (De Bortoli, Natalini, Paluch, & Natalini, 2002). The most commonly-used passive devices include spires to generate turbulent mixing through separation of flow around their edges, fence barriers to increase the height of the boundary layer and floor roughness to develop the velocity deficit near the ground (Cook, 1978; Counihan, 1973). Two different triangular spire designs and timber roughness blocks are shown in Table 1. These dimensions were derived following a theoretical design method outlined by Irwin (1981) such that the height h, base width b and depth d of the spires could be determined based on the desired power law profile with exponent α of 0.2 and boundary layer thickness δ of 1.2 m. Velocity measurements for the two configurations of spire and roughness in Table 1 were taken at different heights using a multi-hole pressure probe and a traverse. The operating conditions of the tunnel were a freestream velocity $U_\infty = 11$ m/s and Reynolds number $Re_\infty = U_\infty \delta / \nu = 8.8\times10^5$.

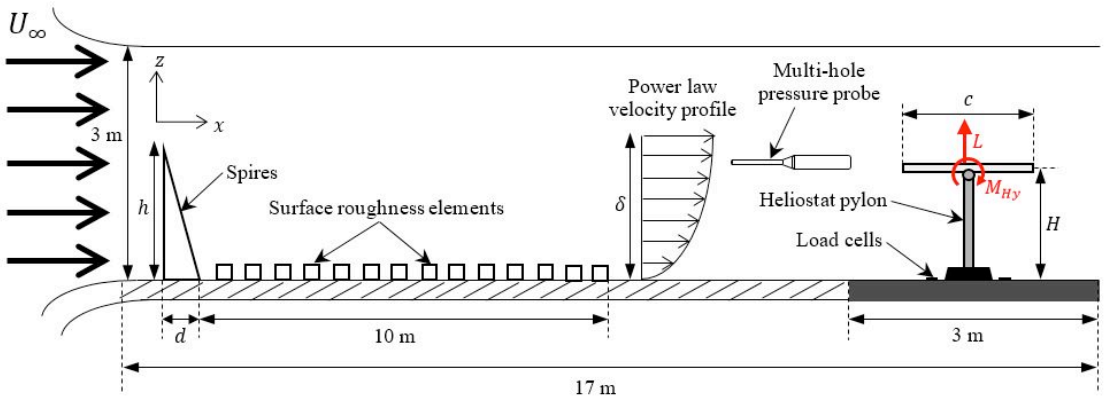

Figure 2: Schematic of the experimental setup for generation of the ABL in the wind tunnel and force measurements on the heliostat model.

Table 1: Dimensions and characteristics of spires and roughness elements

Configuration	Spire height h (m)	Spire base width b (m)	Spire depth d (m)	Roughness width R_b (m)	Roughness height R_h (m)
SR1	1.3	0.155	0.34	0.09	0.045
SR2	1.4	0.2	0.74	0.09	0.045

Figure 3(a) and (b) show the mean velocity and turbulence intensity profiles, respectively, of the two spire and roughness configurations in Table 1. The mean velocity profiles generated by SR1 are within a maximum error of ±5% of a power law ($\alpha = 0.18$) velocity profile. The turbulence intensities generated by SR1 are within ±2% of ESDU 85020 (1985) data for a neutral ABL with a mean wind speed of 10 m/s at a 10 m height, surface roughness height $z_0 = 0.002$ m and boundary layer thickness $\delta = 350$ m. In contrast, the mean velocity profile generated by SR2 is close to linear in the part-depth simulated ABL and generated turbulence intensities above 10%. Hence, the two spire and roughness configurations, SR1 and SR2, can be used to investigate the effect of turbulence intensity on the peak wind loads on the heliostat mirror that was stowed at a range of heights ($0.3 \leq z/\delta \leq 0.5$) indicated by the shaded region in Figure 3.

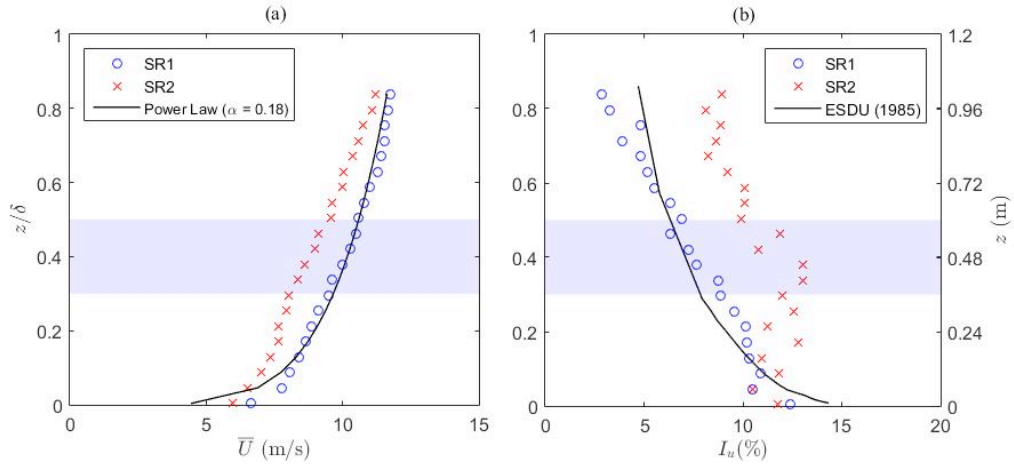

Figure 3: (a) Mean velocity profiles of the two spire configurations compared with the power law profile of a low-roughness terrain; (b) Longitudinal turbulence intensity profiles compared with the ESDU (1985) profile of a low-roughness terrain. The shaded area indicates the heights at which the heliostat mirror was stowed.

Force measurements on the model heliostat were taken using four three-axis load cells, mounted on a rotary turntable in Figure 2. Each load cell has a capacity of 500 N with a sampling frequency of 1 kHz in all three axes and an accuracy of ±0.5% of full scale. The heliostat was modelled as a thin flat plate in the absence of a support structure. A series of six square aluminium plates with 3 mm thickness and chord length (c) ranging from 300 mm to 800 mm were manufactured and mounted on a common pylon with a telescopic design to allow the elevation axis height H of the plate to vary between 0.35 m and 0.6 m. The peak lift force on the plate (L in Figure 2) was determined from the difference between the measured lift forces on the heliostat (plate mounted to pylon) and those on the heliostat pylon in the absence of a mounted plate. The peak hinge moments on the plate (M_{Hy} in Figure 2) were calculated from the product of the peak lift force on the plate and the longitudinal distance from the centre of pressure to the centre of the plate. The peak lift coefficient

and peak hinge moment coefficients on the plate were calculated following Peterka and Derickson (1992) as:

$$c_L = \frac{L}{1/2\rho \bar{U}^2 A} \quad (1)$$

$$c_{M_{Hy}} = \frac{M_{Hy}}{1/2\rho \bar{U}^2 A c} \quad (2)$$

Here ρ (kg/m^3) is the density of air, $\bar{U}$ (m/s) is the mean wind speed at the heliostat elevation axis height H, $A = c^2$ (m^2) is the heliostat mirror area and c is the heliostat chord length.

Results

Figure 4 shows the effect of the heliostat chord length on the peak wind load coefficients on a heliostat in stow position exposed to SR1 and SR2. The peak lift coefficients for SR2 in Figure 4(a) and the peak hinge moment coefficients in Figure 4(b) are approximately double those for SR1. Both the peak lift and peak hinge moment coefficients increase by approximately double as the chord length is halved from 0.8 m to 0.4 m. This indicates that there is an inverse proportionality between the wind load coefficients and the chord length of the heliostat mirror.

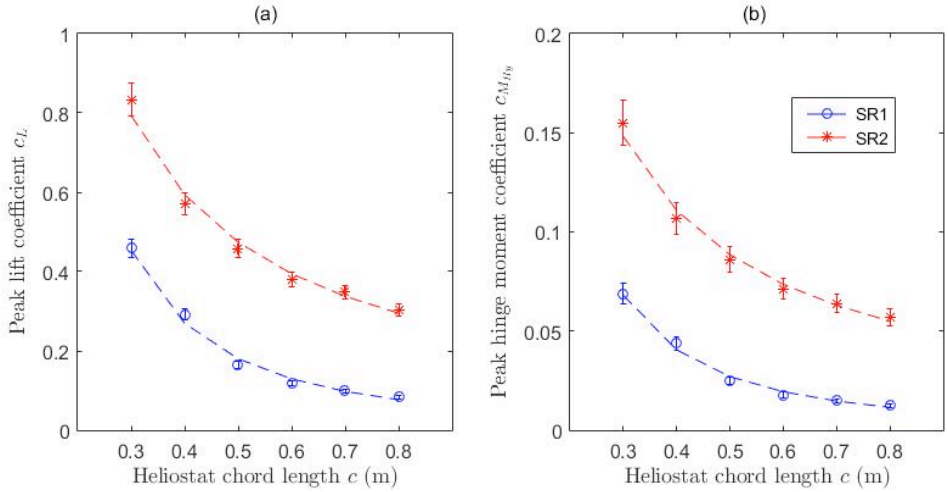

Figure 4: Effect of the heliostat chord length for SR1 and SR2 on (a) peak lift coefficient; (b) peak hinge moment coefficient on a stowed heliostat.

Figure 5 shows the effect of the elevation axis height on the peak wind load coefficients on stowed heliostats of two different chord lengths exposed to SR1. Both the peak lift coefficients in Figure 5(a) and the peak hinge moment coefficients in Figure 5(b) increase linearly with the elevation axis height of the heliostat. Hence, the peak wind load coefficients can be reduced by 21% and 23% for chord lengths of 0.5 m and 0.8 m, respectively, by lowering the elevation axis height of the heliostat by 30%.

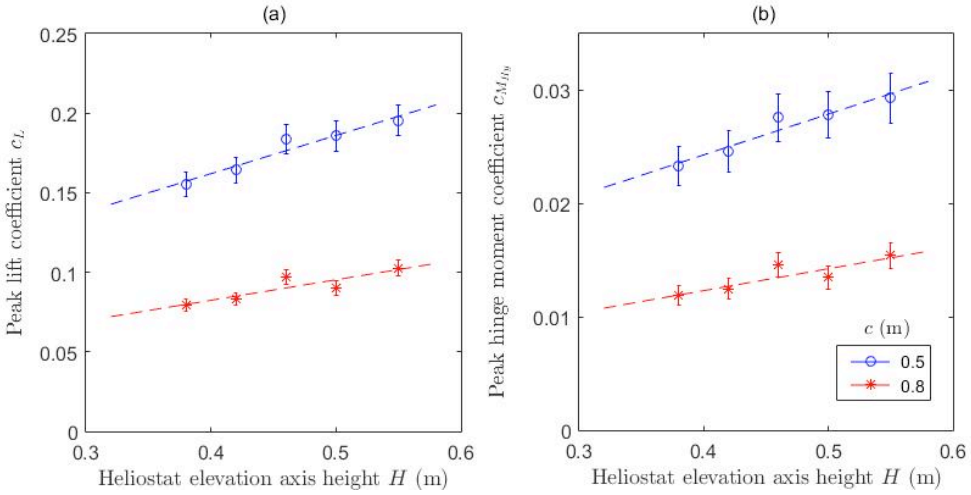

Figure 5: Effect of the heliostat elevation axis height for SR1 on (a) peak lift coefficient; (b) peak hinge moment coefficient on a stowed heliostat.

Figure 6 shows the effect of the outer diameter and thickness of the heliostat pylon for a heliostat mirror with chord length of 0.8 m stowed at different elevation axis heights and exposed to SR1. Both the peak lift coefficient (Figure 6(a)) and the peak hinge moment coefficient (Figure 6(b)) can be reduced by approximately 10% by increasing the outer diameter of the pylon from 33 mm to 42 mm and increasing the thickness of the pylon from 5 mm to 6 mm.

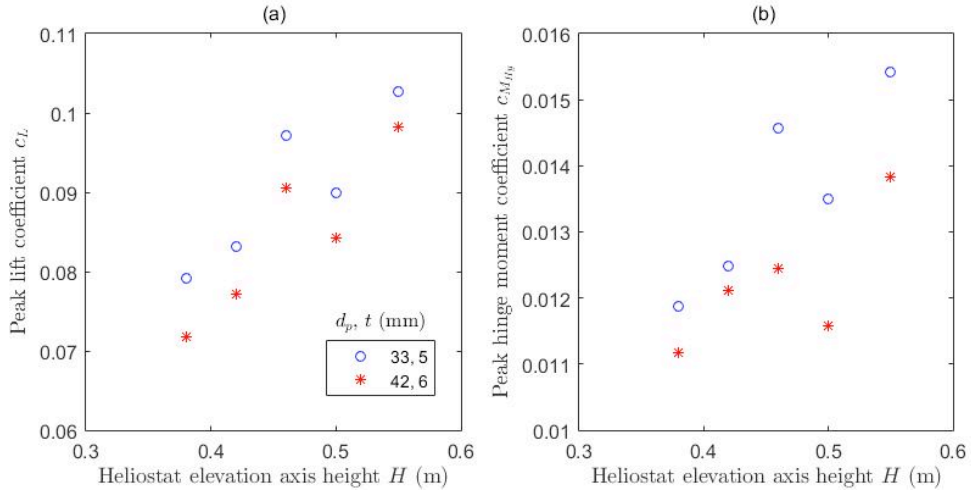

Figure 6: Effect of the heliostat pylon diameter on (a) peak lift coefficient; (b) peak hinge moment coefficient on a stowed heliostat with a chord length of 0.8 m.

Figure 7 shows the effect of longitudinal turbulence intensity on the peak wind load coefficients for comparison with the coefficients reported by Pfahl et al. (2015) at a turbulence intensity of 13%. At a similar turbulence intensity of 12.5%, the peak lift coefficient (Figure 7(a)) and peak hinge moment coefficient (Figure 7(b)) on the heliostat with chord length of 0.5 m in the current study were 13% and 23% lower, respectively than those measured by Pfahl et al. (2015). The pronounced linear increase of the peak wind load coefficients on stowed heliostats at turbulence intensities larger than 10% in the current study is in agreement with a similar finding

by Peterka, Tan, Cermak, and Bienkiewicz (1989) for the peak drag and lift coefficients on heliostats in operating positions.

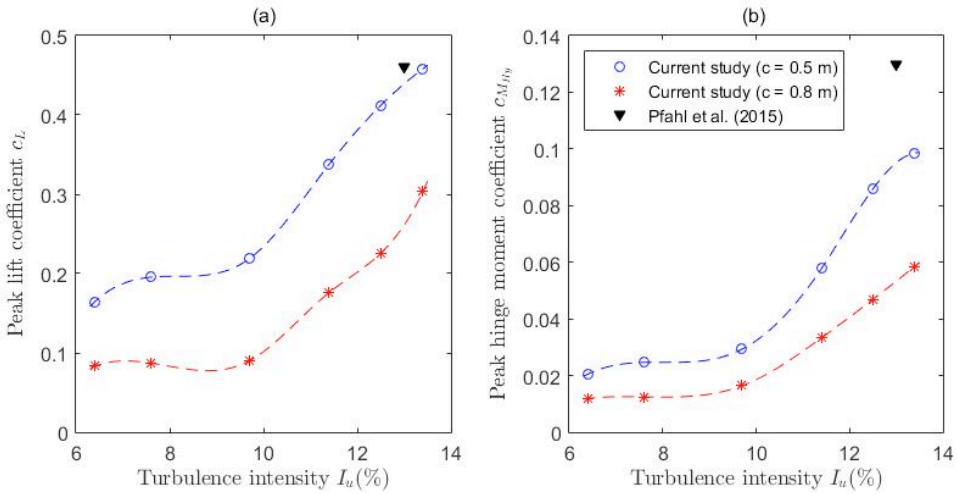

Figure 7: Effect of longitudinal turbulence intensity on (a) peak lift coefficient; (b) peak hinge moment coefficient on a stowed heliostat.

Conclusions

The effect of the critical scaling parameters of a heliostat on the peak lift coefficient and peak hinge moment coefficient on a stowed heliostat was investigated using force measurements on different-sized plates at a range of elevation axis heights. Peak wind load coefficients showed an inverse proportionality with the chord length of the heliostat mirror, so that a halving of the mirror chord length resulted in a doubling of the coefficients. This suggests that the coefficients can be optimised by increasing the size of the heliostat mirror relative to the sizes of the relevant eddies approaching the heliostat. The peak lift coefficient and peak hinge moment coefficient on the stowed heliostat could be reduced by 21% and 23%, respectively, by lowering the elevation axis height of the heliostat mirror by 30% in the simulated ABL. In comparison, the peak wind load coefficients were reduced by less than 10% with an increase in the outer diameter and thickness of the heliostat pylon. A significant linear increase of the peak wind load coefficients occurred at longitudinal turbulence intensities greater than 10% in the simulated ABL. Hence, the peak wind loads on stowed heliostats during high-wind conditions in the ABL are highly sensitive to the critical scaling parameters of the heliostat and should be carefully considered depending on the turbulence characteristics of the site. Optimisation of the ultimate design wind loads can lead to cost reductions in the manufacturing of heliostats from lower strength and lighter materials.

Acknowledgements

Support for the work has been provided by the Australian Government Research Training Program Scholarship and by the Australian Solar Thermal Research Initiative (ASTRI) through funding provided by the Australian Renewable Energy Agency (ARENA).

References

Cook, N. J. (1978). Determination of the model scale factor in wind-tunnel simulations of the adiabatic atmospheric boundary layer. *Journal of Wind Engineering and Industrial Aerodynamics,* 2(4), 311-321.

Counihan, J. (1973). Simulation of an adiabatic urban boundary layer in a wind tunnel. *Atmospheric Environment,* 7(7), 673-689.

Coventry, J., & Pye, J. (2014). Heliostat cost reduction–where to now? *Energy Procedia,* 49, 60-70.

De Bortoli, M., Natalini, B., Paluch, M., & Natalini, M. (2002). Part-depth wind tunnel simulations of the atmospheric boundary layer. *Journal of Wind Engineering and Industrial Aerodynamics,* 90(4), 281-291.

Emes, M. J., Arjomandi, M., & Nathan, G. J. (2015). Effect of heliostat design wind speed on the levelised cost of electricity from concentrating solar thermal power tower plants. *Solar Energy,* 115, 441-451.

Hernández-Moro, J., & Martínez-Duart, J. M. (2012). CSP electricity cost evolution and grid parities based on the IEA roadmaps. *Energy Policy,* 41, 184-192.

Hinkley, J. T., Hayward, J. A., Curtin, B., Wonhas, A., Boyd, R., Grima, C., . . .

Naicker, K. (2013). An analysis of the costs and opportunities for concentrating solar power in Australia. *Renewable Energy,* 57, 653-661.

IEA-ETSAP, & IRENA. (2013). *Concentrating Solar Power Technology Brief*.

IRENA. (2013). Renewable Power Generation Costs in 2012: An Overview. *Bonn, Germany.*

IRENA. (2015). The Power to Change: Solar and Wind Cost Reduction Potential to 2025. *Bonn, Germany.*

Irwin, H. (1981). The design of spires for wind simulation. *Journal of Wind Engineering and Industrial Aerodynamics,* 7(3), 361-366.

Kolb, G. J., Ho, C. K., Mancini, T. R., & Gary, J. A. (2011). *Power Tower Technology Roadmap and Cost Reduction Plan* (SAND2011-2419). Albuquerque, USA.

Kolb, G. J., Jones, S. A., Donnelly, M. W., Gorman, D., Thomas, R., Davenport, R., & Lumia, R. (2007). *Heliostat Cost Reduction Study* (SAND2007-3293). Albuquerque, USA.

Lovegrove, K., & Stein, W. (2012). *Concentrating solar power technology: principles, developments and applications*. Cambridge, UK: Woodhead Publishing Limited.

Peterka, J. A., & Derickson, R. G. (1992). *Wind load design methods for ground-based heliostats and parabolic dish collectors* (SAND92-7009). Albuquerque, USA.

Peterka, J. A., Tan, Z., Cermak, J. E., & Bienkiewicz, B. (1989). Mean and peak wind loads on heliostats. *Journal of Solar Energy Engineering,* 111(2), 158-164.

Pfahl, A., Randt, M., Meier, F., Zaschke, M., Geurts, C., & Buselmeier, M. (2015). A holistic approach for low cost heliostat fields. *Energy Procedia,* 69, 178-187.

Contact email: matthew.emes@adelaide.edu.au